© 2017. Published by The Company of Biologists Ltd | Journal of Cell Science (2017) 130, 1224-1231 doi:10.1242/jcs.189316

SHORT REPORT

Attenuation of N-glycosylation causes polarity and adhesion defects in the *C. elegans* embryo

Julia Stevens and Anne Spang*

ABSTRACT

The *Caenorhabditis elegans* early embryo is highly polarized, requiring sequestration of cytoplasmic polarity factors at the plasma membrane. This compartmentalization aids asymmetric distribution of lipids and proteins, which is partially responsible for the fates of the daughter cells. Since most plasma membrane proteins are glycosylated, we determined the effect of attenuation of N-glycosylation on cell polarity. While polarity establishment was not perturbed, the size difference between the two cells formed in first cell division (AB and P1) was more variable in embryos with reduced N-glycosylation than in the mock-treated embryos. In addition, among other deficiencies, we observed spindle orientation defects in two-cell embryos. Moreover, cell–cell adhesion was specifically lost at the two-cell stage when N-glycosylation was reduced. This loss-of-adhesion phenotype was rescued by interfering with polarity establishment, indicating that polarity establishment enforces plasma membrane compartmentalization. Consistent with this idea, the decreased plasma membrane levels of the adhesion proteins E-cadherin and MAGI-1 in *ribo-1(RNAi)* embryos were restored in the absence of functional PAR-2. Our data suggest a general role for N-glycosylation in plasma membrane compartmentalization and cell polarity.

KEY WORDS: *C. elegans*, N-glycosylation, PAR protein, Cell adhesion, Cell polarity, Embryo development, Membrane compartmentalization, E-cadherin, OST complex

INTRODUCTION

Establishment and maintenance of cell polarity are essential in development. They provide the means of body axis formation and determine cell fate decisions. Moreover, many differentiated cells, such as neurons and epithelial cells, maintain an intrinsic polarity, which is essential for cellular functionality. In early development in many organisms, as well as in epithelial cells, Par proteins are key in the establishment and maintenance of cell polarity. One of the best-characterized models for cell polarity is the *Caenorhabditis elegans* embryo (Motegi and Seydoux, 2013). In the zygote, a complex of PAR-3, PAR-6 and atypical protein kinase C (aPKC) lines the cortex. Upon fertilization, PAR-2 is recruited to the cortex at the site of sperm entry, which marks the posterior pole. The PAR-2 domain expands, replacing the anterior complex of PAR-3, PAR-6 and aPKC. Finally, in a tug-of-war, the boundary and the size of the anterior and posterior domains are established. Interestingly, defects in domain size can be corrected at later stages before cell division (Schmutz et al., 2007; Schonegg et al., 2007).

Biozentrum, University of Basel, Klingelbergstrasse 70, Basel CH-4056, Switzerland.

*Author for correspondence (anne.spang@unibas.ch)

A.S., 0000-0002-2387-6203

Received 11 March 2016; Accepted 6 February 2017

Neither of the PAR proteins nor aPKC contain a transmembrane domain, and the complexes are recruited to the plasma membrane through lipid interactions (Goehring et al., 2011; Motegi and Seydoux, 2013). However, it is unknown whether plasma membrane proteins play an essential role in the cortical localization of PAR proteins and thereby contribute to polarity establishment and maintenance in the early embryo. Most plasma membrane proteins are glycosylated. Knockdown of a xylosyltransferase, which is involved in chain extension of O-glycosylated proteins, did not affect polarity establishment but caused a cytokinesis defect (Wang et al., 2005). Therefore, we decided to concentrate on N-glycosylated proteins and to attenuate N-glycosylation through depletion of oligosaccharyl transferase (OST) complex activity. Over 80% of plasma membrane proteins are N-glycosylated in the ER, and this modification is essential for protein folding, function and stability. We have previously shown that depletion of OST complex components leads to secretion defects (Stevens and Spang, 2013). Here, we report that N-glycosylation is important for cell adhesion and cell polarity, suggesting a role for N-glycosylated proteins in the compartmentalization of the plasma membrane.

RESULTS AND DISCUSSION

Polarity establishment is normal in *ribo-1(RNAi)* zygotes

The PAR-3–PAR-6–aPKC complex and PAR-2 are soluble and are recruited to the cell cortex through lipid and protein interactions. To evaluate the role of proteins residing in the plasma membrane in polarity establishment, we reduced the amount of N-glycosylation by depleting a member of the OST complex, *ribo-1* [by performing RNAi experiments, denoted *ribo-1(RNAi)*], and assessed cell polarity in the zygote (Fig. 1A). mCherry::PAR-6 and GFP::PAR-2 were localized at the plasma membrane in the anterior and posterior portion of the cells, respectively, at the metaphase–anaphase transition in both mock and *ribo-1(RNAi)*-treated zygotes. In contrast, as reported previously (Rappleye et al., 1999), depletion of the coronin-like protein POD-1, decreased PAR-2 recruitment to the cell cortex (Fig. 1A). Our data suggest that N-glycosylation of proteins may not be critical for initial polarity establishment in the *C. elegans* zygote.

ribo-1(RNAi) increases the variability of the AB:P1 cell-size ratio

In the above experiment, we noticed that, after the first cell division, the difference in cell size between the AB and P1 cells was often less prominent in *ribo-1(RNAi)* compared to mock-treated embryos. As observed previously (Schierenberg and Wood, 1985), the AB:P1 size ratio is rather constant in wild-type two-cell embryos, and the AB cell is about 1.4× larger than the P1 cell (Fig. 1B). In *ribo-1(RNAi)* embryos, the variance of the AB:P1 ratio is much larger than in the mock-treated control, and the average ratio is smaller. *ribo-1(RNAi)* early embryos are also exquisitely sensitive to light. To ensure that the

Journal of Cell Science

Journal of Cell Science (2017) 130, 1224-1231 doi:10.1242/jcs.189316

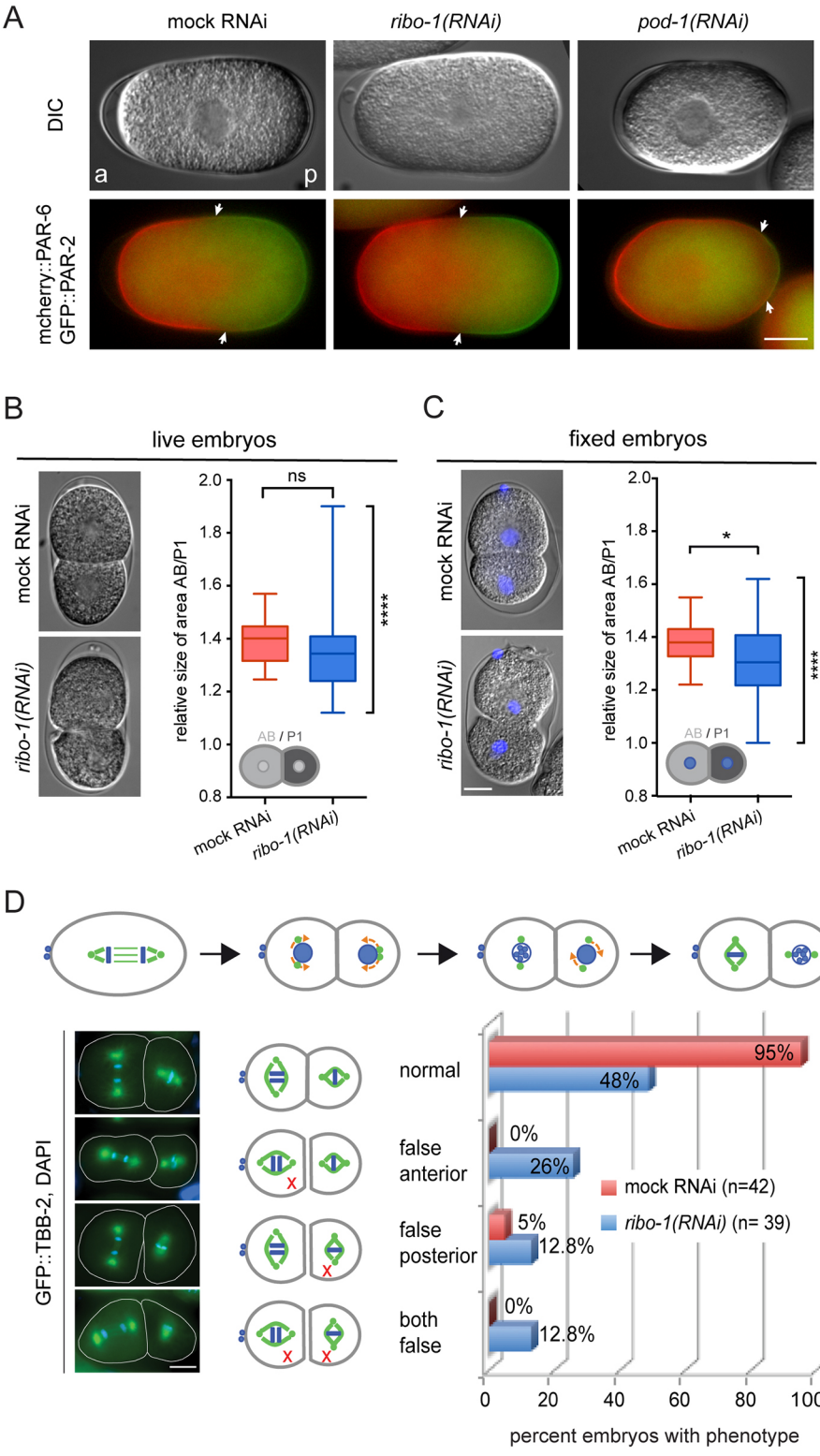

Fig. 1. N-glycosylation is required for cell polarity. (A) Live-cell imaging of mock-treated, and *ribo-1(RNAi)* or *pod-1(RNAi)* one-cell embryos expressing mCherry::PAR-6 and GFP::PAR-2. a, anterior; p, posterior; same orientation for all embryos. Arrows point to domain boundaries. 100% of the analyzed embryos [mock=9; *ribo-1(RNAi)*=22; *pod-1(RNAi)*=8] showed the depicted phenotype. (B) Quantification of the AB:P1 size ratio in ≥40 live embryos imaged under pressure-free and isosmotic conditions. (C) Example images and quantification of the AB:P1 size ratio of 50 fixed embryos. DNA was stained with DAPI. In the box plots, the box represents the 25–75th percentiles, and the median is indicated. The whiskers show the minimum to maximum range. (D) Mitotic spindles orientation failures in *ribo-1(RNAi)* two-cell embryos. Fixed DAPI-stained GFP::TBB-2 two-cell embryos were classified. A wild-type progression is shown at the top. Scale bars: 10 µm. *P<0.05; ****P<0.0001; ns, not significant (unpaired two-tailed t-test with Welch's correction).

apparent cell size changes were not due to an artifact introduced by the imaging method, we repeated the analysis with fixed embryos (Fig. 1C), and found that this experiment gave same results. Thus, although polarity establishment is not perturbed, the cell size ratio cannot be properly maintained in *ribo-1(RNAi)* embryos. This is surprising because, in some instances, like upon the depletion of the Rho GTPase-activating proteins (GAPs) RGA-3 and RGA-4, the anterior–posterior domain sizes are not set up properly, yet this defect is corrected before cell division (Schmutz et al., 2007; Schonegg et al., 2007). It is tempting to speculate that even though the localization of the PAR proteins is not disturbed, the function of PAR complexes might be somewhat impaired. Alternatively, reduced N-glycosylation may compromise spindle positioning and therefore the division plane position may be more variable.

Journal of Cell Science

Journal of Cell Science (2017) 130, 1224-1231 doi:10.1242/jcs.189316

ribo-1(RNAi) embryos have spindle orientation defects

We next tested whether this variability in cell size has any consequence for subsequent cell divisions. The AB cell is not only bigger than P1 but also enters mitosis first. Thus, there is not only spatial but also temporal asymmetry in the two-cell stage embryo. Moreover, the mitotic spindle rotates by 90° in P1, yielding perpendicular division planes of AB and P1 (Fig. 1D). We investigated the division pattern in the two-cell embryo by using tubulin fused to GFP (GFP::TBB-2) and DAPI to mark the spindle and DNA, respectively. In 26% of the embryos, we obtained a spindle rotation defect reminiscent of the one observed in *par-3* mutants, and in ∼13% one similar to *par-2* mutants (Kemphues et al., 1988) (Fig. 1D). In another ∼13%, the orientation was inverted. However, unlike in *par* mutants, the timing of entering mitosis in AB and P1 cells appeared to be normal in *ribo-1(RNAi)* embryos, suggesting that only the spatial but not the temporal asymmetry was affected. These data indicate that the cues for spindle rotation and cell cycle progression are separable.

ribo-1(RNAi) causes loss-of-adhesion specifically after the first cell division

We have reported previously that reduced N-glycosylation leads to severe cytokinesis defects and delayed development (Stevens and Spang, 2013). The embryos that were able to successfully complete cytokinesis under those conditions, lost the adhesion between AB and P1 cells (Fig. 2A; Fig. S1). Adhesion failed only once, as in subsequent cell divisions, cell adhesion was maintained, and two separate cell masses developed in ∼50% of the *ribo-1(RNAi)* embryos, as indicated by the cleft between the cell masses (Fig. 2A,B). To ensure that the adhesion failure was specific to attenuated N-glycosylation and not due to eggshell formation defects and osmo-sensitivity, we fixed embryos expressing the plasma membrane marker PH(PLC)::GFP (Varnai et al., 2002). The adhesion phenotype was even more readily detectable after fixation and was independent of osmo-sensitivity or general secretion defects (Fig. 2B). Neither depletion of the plasma membrane t-SNARE SYX-4 (Jantsch-Plunger and Glotzer, 1999) nor *pod-1(RNAi)* triggered a similar cleft between AB and P1 cells or a separation of cell masses at later stages of embryonic development (Fig. 2B), in spite of producing osmo-sensitive embryos (Sönnichsen et al., 2005; data not shown). Thus, the observed adhesion failure is not connected to osmo-sensitivity or general secretion defects, making simple plasma membrane damage an unlikely explanation for the observed phenotypes. We conclude that N-glycosylation is required for proper cell adhesion specifically after the first cell division, and that this lack of adhesion may also contribute to the aberrant spindle positioning at the two-cell stage. Interestingly, in subsequent cell divisions, cell–cell adhesion was not affected to the same extent. One likely explanation is that OST complexes present in sperm, which is resistant to RNAi, provides enough N-glycosylation activity to restore adhesion capabilities in later divisions.

The plasma membrane of the posterior and anterior cell masses have different properties

The two cell masses observed in *ribo-1(RNAi)* embryos possessed different morphological features, in that the anterior cell mass had a relatively smooth surface, while the posterior cell mass had a rougher appearance (Fig. 2A,C); the phenotype was more obvious in later stages of development. Moreover, in ∼10–15% of the embryos, the lipophilic dye FM4-64 penetrated the posterior cell mass much more readily than the anterior cell mass, indicating that the plasma membrane composition in the two cell masses might be different in *ribo-1(RNAi)* embryos (Fig. 2C). In contrast, no such distinction was observed in wild-type embryos in which we punctured the eggshell to allow FM4-64 to penetrate. Thus, the physicochemical properties appear to be different between the anterior and posterior cell masses, consistent with an overall alteration in the composition of the plasma membrane.

Loss of polarity establishment rescues the cell adhesion phenotype of *ribo-1(RNAi)*

This difference in FM4-64 permeability described above could already be observed at the two-cell stage (Fig. 2C, top panel). We hypothesized that unequal segregation of proteins at the plasma membrane could be the underlying cause of the adhesion defect. To test this hypothesis, we eliminated polarity establishment through depletion of the cell polarity protein PAR-2. *ribo-1(RNAi) par-2(RNAi)* restored adhesion between the AB and P1 cells, as fewer embryos with a cleft were observed (Fig. 3A,B). As expected, *par-2(RNAi)* did not rescue nor cause osmo-sensitivity, as indicated by the inability of FM4-64 to reach the interior of the egg. Consistent with this, impairment of polarity establishment through PAR-6 depletion increased adhesion between cells in *ribo-1(RNAi)* embryos, while knockdown of two unrelated genes did not alter the *ribo-1(RNAi)* adhesion defect (Fig. 3B). Similar results were obtained with temperature-sensitive *par-2* and *par-4* alleles (Fig. 3C,D; Fig. S2). Thus, the adhesion failure caused by RIBO-1 depletion can be rescued by interfering with cell polarity, whether the embryo cell takes on an anterior fate [*par-2(RNAi)*] or posterior [*par-6(RNAi)*] cell fate (Fig. 3B). This suggests that polarization of the embryo, and hence compartmentalization, the plasma membrane might be the cause of the adhesion defect.

Interfering with polarity in multiple ways rescues the cell adhesion defects of *ribo-1(RNAi)*

If the above interpretation is correct, knockdown of any component involved in cell polarity in the one-cell embryo should rescue the *ribo-1(RNAi)*-induced adhesion defect. To test this hypothesis, we depleted factors acting downstream of polarity establishment. *PPK-1* is a phosphoinositide 5-kinase that is important for asymmetric spindle position in the one-cell embryo (Panbianco et al., 2008). *ppk-1(RNAi)* rescued the adhesion phenotype caused by *ribo-1 (RNAi)* (Fig. 3E). Similar results were obtained upon depletion of POD-1, or RGA-3 and RGA-4. The observed rescues were not due to a dilution effect of the double knockdown, as *ribo-1* mRNA levels were reduced to ∼20% under all conditions (Fig. S3B). Our data are consistent with the notion that interfering with cell polarity rescues *ribo-1(RNAi)*-induced loss of adhesion after the first cell division.

Taken together, our data show that attenuation of N-glycosylation through knockdown of RIBO-1 affects adhesion at the two-cell stage. We have shown previously that, under these conditions, the concentration of the plasma membrane-localized yolk receptor RME-2 is strongly reduced (Stevens and Spang, 2013), suggesting that the concentration of plasma membrane proteins in general might be reduced in *ribo-1(RNAi)* zygotes. Upon fertilization and, hence, establishment of plasma membrane domains in the zygote, the protein concentration might be too low to provide a sufficient density of proteins in the different domains (Fig. 4G). Alternatively, it is possible that only fewer or smaller domains can be established and/or maintained. A prediction from both possibilities is that the level of adhesion molecules at cell–cell contacts would be reduced.

Journal of Cell Science

Journal of Cell Science (2017) 130, 1224-1231 doi:10.1242/jcs.189316

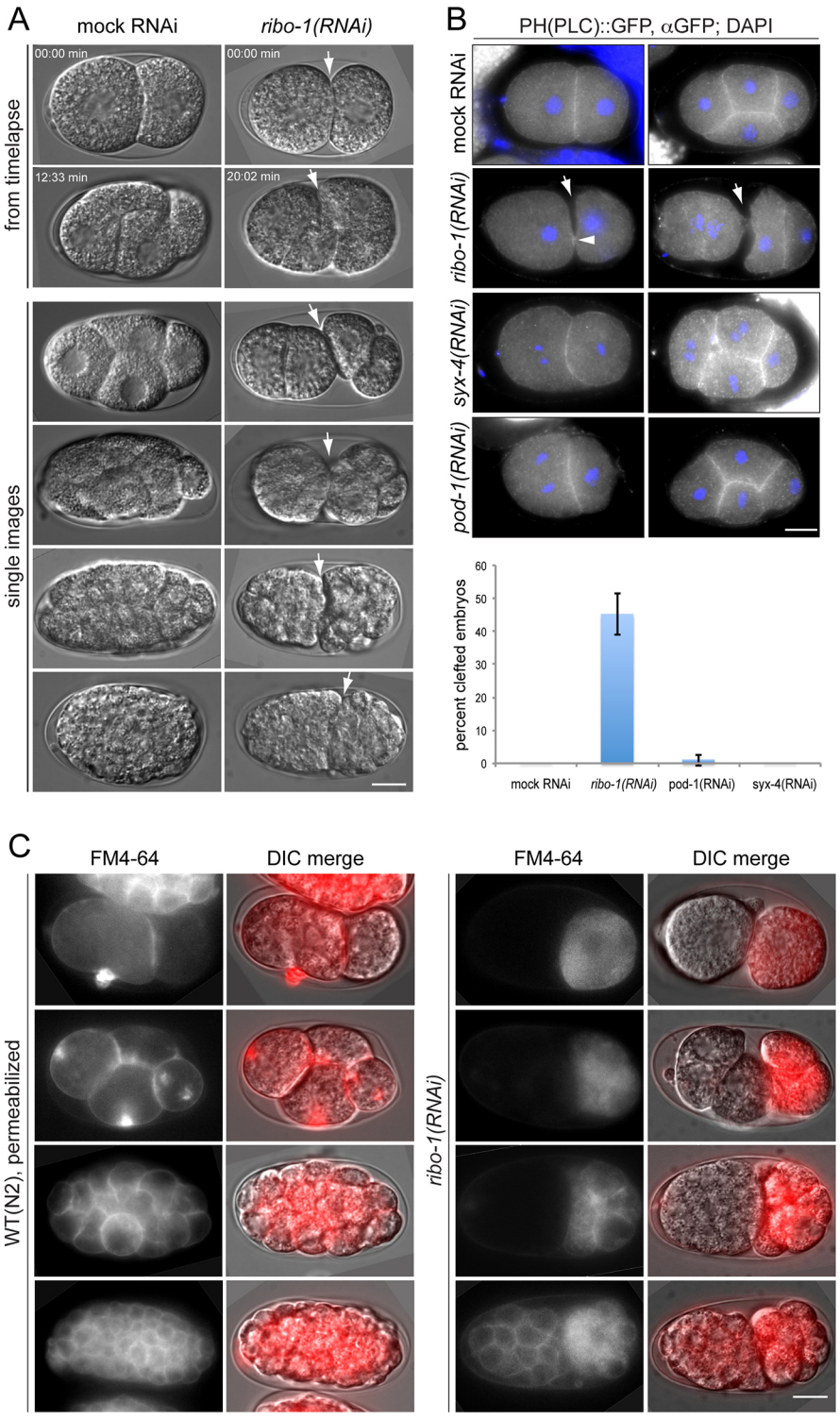

Fig. 2. N-glycosylation is required for cell adhesion and membrane compartmentation. (A) Differential interference contrast (DIC) images from either a time-lapse or individual images. The arrows point to the cleft in *ribo-1(RNAi)* embryos. (B) Fixed and stained PH(PLC)::GFP-expressing embryos. Arrows indicate the cleft; the arrowhead points to the midbody. A quantification of the phenotype (mean±s.d.) is shown underneath (≥220 embryos from three or more experiments were analyzed per condition). (C) FM4-64 staining. Untreated eggs were permeabilized with an injection capillary prior to staining. WT, wild-type. Scale bars: 10 µm.

MAGI-1 and HMR-1 plasma membrane localization in *ribo-1 (RNAi)* embryos depends on polarity factors

The conserved cell–cell junction scaffold protein MAGI-1 is expressed in one-cell embryos (Hillier et al., 2009) and localized to cell-contact sites of two-cell embryos (Fig. 4A). Consistent with our prediction, the MAGI-1 signal was drastically reduced at the cleft in *ribo-1(RNAi)* embryos and restored in *par-2(RNAi) ribo-1 (RNAi)* embryos (Fig. 4A). Like MAGI-1, the *C. elegans* E-cadherin HMR-1 is expressed in the one-cell embryo (Hillier et al., 2009; Munro et al., 2004). *ribo-1(RNAi)* significantly reduced E-cadherin staining at the plasma membrane (Fig. 4B,C). This effect was reversed when polarity was also perturbed. As expected, knockdown of SYX-4 or POD-1 had no gross effect on the localization of MAGI-1 or HMR-1 (Fig. 4A–C).

Recently, a line in which HMR-1 was chromosomally appended with GFP was reported (Marston et al., 2016). In this strain, E-cadherin is detectable at the AB–P1 cell contact site (Fig. 4D). Consistent with the immunofluorescence data, we detected less E-cadherin in *ribo-1(RNAi)* embryos than in mock-treated or *par-2 (RNAi) ribo-1(RNAi)* embryos (Fig. 4D,E). The remaining signal

Journal of Cell Science

Journal of Cell Science (2017) 130, 1224-1231 doi:10.1242/jcs.189316

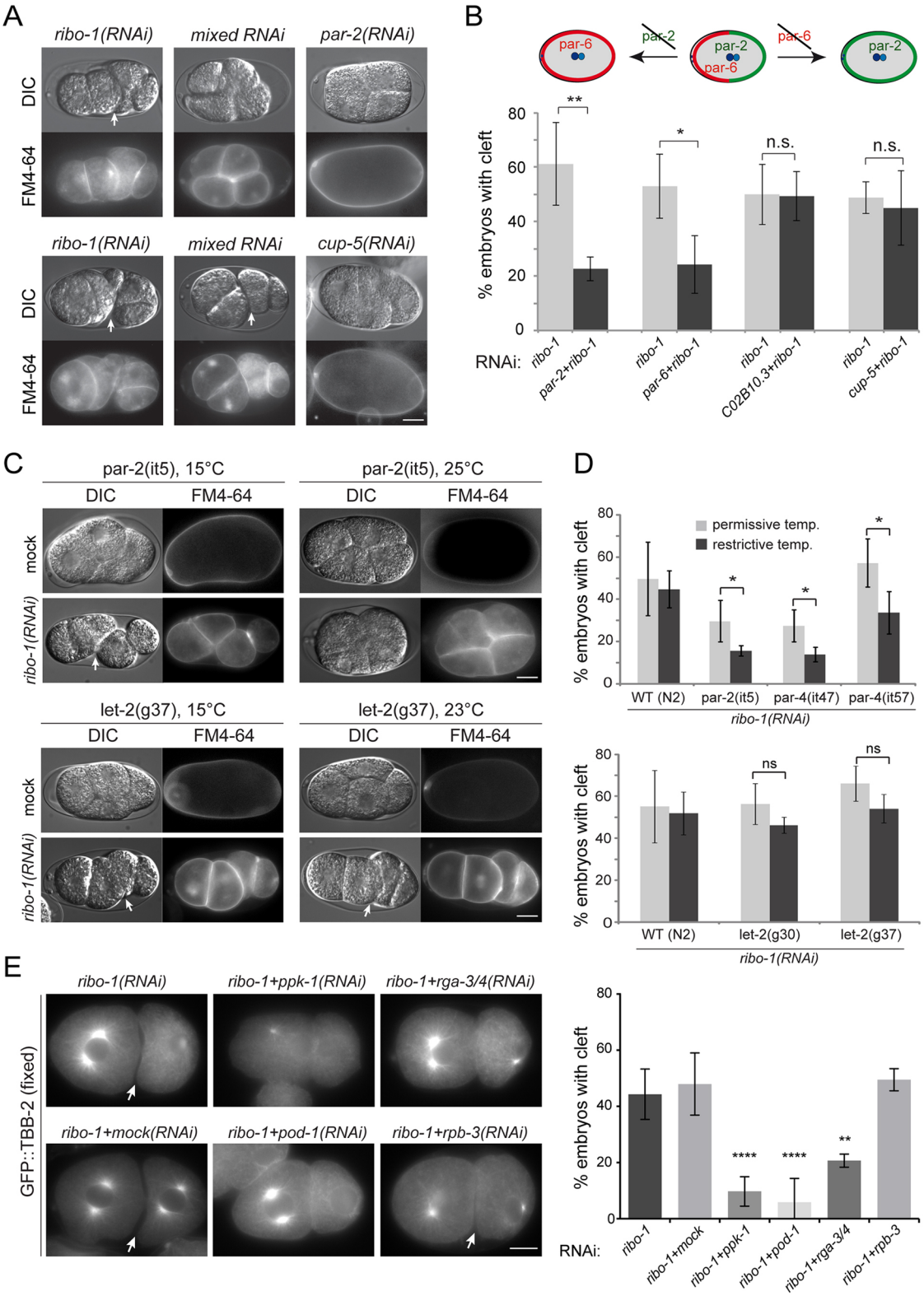

Fig. 3. Loss of polarity rescues the *ribo-1(RNAi)* adhesion phenotype. (A) Depletion of PAR-2 or CUP-5 individually or together (mixed RNAi) with *ribo-1 (RNAi)*. Egg shell permeability was assessed by FM4-64 staining. (B) Quantification of the experiments shown in A and additional knockdown combinations. For each condition, ≥270 embryos from three or more experiments were analyzed. A schematic of the *par-2 and par-6* mutant phenotypes is shown above the graph. (C) *par-2* and *par-4* temperature-sensitive mutants also rescue the *ribo-1(RNAi)* phenotype when raised at the restrictive temperature. (D) Quantification of the cleft phenotype shown in C. For each condition, ≥170 embryos from three or more experiments were analyzed. (E) Depletion of various polarity proteins rescued the *ribo-1(RNAi)* phenotype. Individual or double RNAi in embryos expressing GFP::TBB-2. DNA was stained with DAPI. The quantification is for ≥160 embryos from three or more experiments. Results in B, D and E are mean±s.d. **P*<0.05; ***P*<0.01; *****P*<0.0001; ns, not significant (one-way ANOVA and Dunnet's multiple comparisons test). Arrows in A, C and E indicate the cleft. Scale bars: 10 µm.

Journal of Cell Science

Journal of Cell Science (2017) 130, 1224-1231 doi:10.1242/jcs.189316

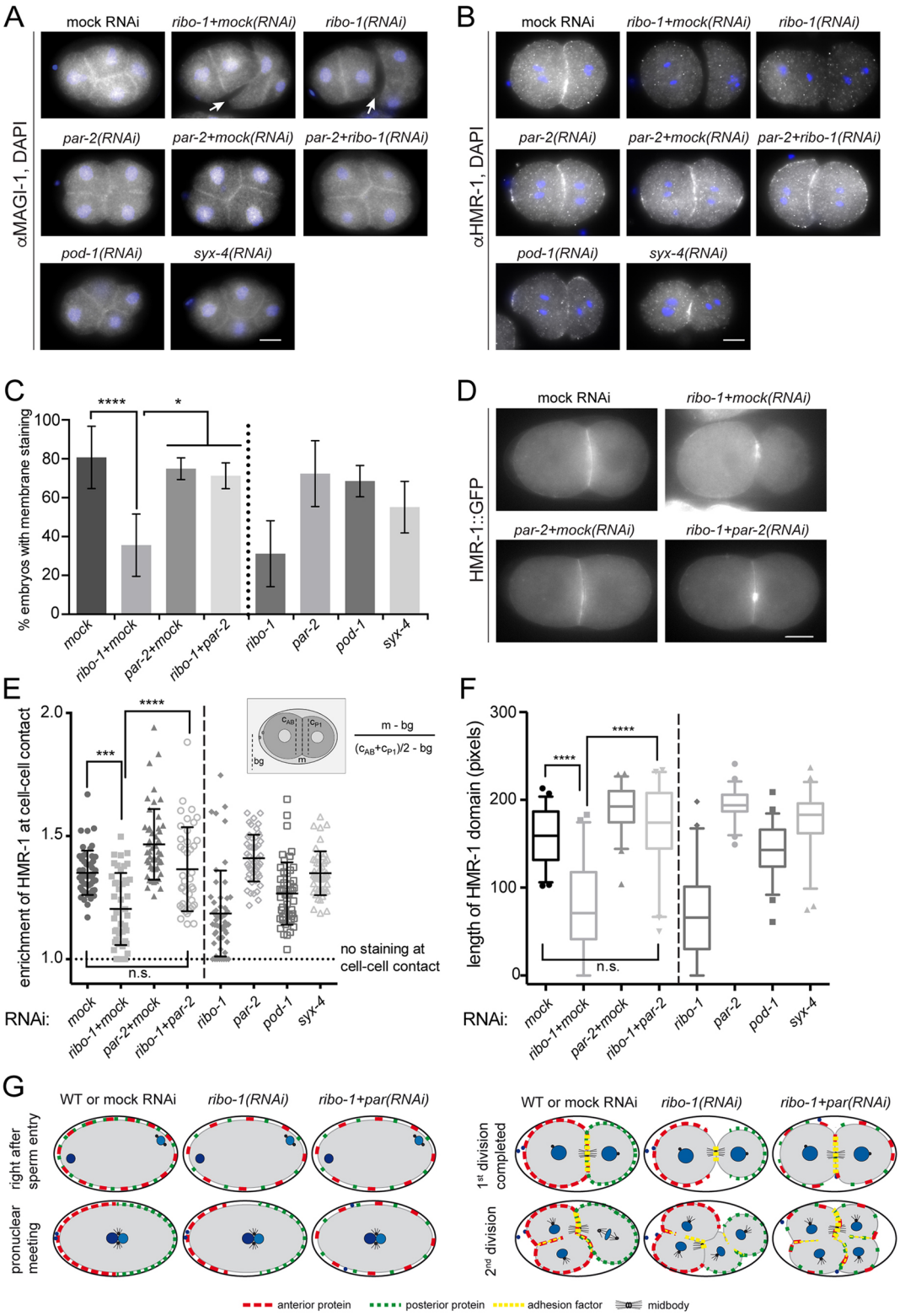

Fig. 4. Proper adhesion molecule localization is dependent on RIBO-1. Immunofluorescence of MAGI-1 (A) and HMR-1 (B) in various single and double knockdowns. DNA was stained with DAPI. Arrows indicate the cleft. (C) Quantification (mean±s.d.) of results in B; ≥55 embryos from three or more experiments were analyzed. *P<0.05; ****P<0.0001 (one-way ANOVA and Tukey's multiple comparisons test). (D) Live imaging of two-cell HMR-1::GFP embryos under pressure-free isosmotic conditions. (E,F) Quantification of the length of the HMR-1 domain (E) and of the relative amount of HMR-1::GFP (F) at cell–cell contacts. A 10 pixel-wide segmented line was drawn along the visible HMR-1 domain, then displaced into the cytoplasm of both cells and into the slide background, and for each location the mean gray value and the length was recorded. E shows the mean±s.d.; in the box plots in F, the box represents the 25–75th percentiles, and the median is indicated. The whiskers show the 5–95th percentiles. ≥40 two-cell stages from three or more experiments were analyzed. ***P<0.001; ****P<0.0001; ns, not significant (Kruskal–Wallis and Dunn's multiple comparisons tests). (G) Model that explains the adhesion defect in ribo-1(RNAi) embryos and its rescue by loss of cell polarity. For detailed explanation, see text. Scale bars: 10 µm.

Journal of Cell Science

was in the midbody region, which we often observed in fixed embryos to be the only area with residual adhesion. Moreover, the length of the contact site between AB and P1 was strongly reduced (Fig. 4D,F). Thus, less adhesion molecules are present at the plasma membrane in *ribo-1(RNAi)* embryos, and this phenotype is rescued by loss of cell polarity. Yet, *hmr-1(RNAi)* does not phenocopy the adhesion defect of *ribo-1(RNAi)* embryos (Costa et al., 1998; Klompstra et al., 2015; our unpublished data). However, innexins also contribute to adhesion in the early embryo (Bossinger and Schierenberg, 1992). Depletion of innexins in different combinations equally failed to reproduce the *ribo-1(RNAi)*-induced adhesion defect (J.S., unpublished data). It appears that adhesion in the early embryo is rather complex and cannot be easily destroyed.

Finally, we addressed why the AB–P1 cell adhesion defect was not rescued in later divisions, in which cell–cell contacts were established. We recorded short time-lapse movies focusing on the AB division. In mock-treated embryos, the E-cadherin signal was seen to take up a compact location towards the AB cytokinesis furrow, while new E-cadherin was secreted into the Aba–ABp cleavage furrow (Fig. S4; Movies 1 and 2). In contrast, in *ribo-1(RNAi)* embryos, the E-cadherin domain 'slid over' to the AB cytokinesis furrow and contributed, with the newly deposited E-cadherin, to cell adhesion, while there was essentially no E-cadherin left at the AB–P1 contact site (Fig. S4; Movies 3–8). These data indicate that after the completion of cytokinesis, secretion to the AB–P1 boundary stops, and new secretion sites are presumably formed at the next cytokinesis sites (Fig. 4G). Taken together, our data reveal an unexpected interplay between N-glycosylation, membrane compartmentalization, cell adhesion and cell polarity.

MATERIALS AND METHODS

General methods and strains

C. elegans was cultured and maintained as described previously (Brenner, 1974) at 20°C. Strains KK114 [daf-7(e1372) par-2(it5)III], KK184 [par-4 (it47)V], KK300 [par-4(it57)V] (Ken Kemphues, Cornell University, Ithaka, USA), GG30 [let-2(g30)X, GG37 (let-2(g37)X] (Gunter von Ehrenstein, MPI Göttingen, Germany) and WH204 {unc-119(ed3) III; ojIs1 [*pie-1::GFP::tbb-2+unc-119(+)*]} (Strome et al., 2001) were obtained from the *Caenorhabditis* Genetics Center (CGC) and TH120 ([*pie-1::GFP::par-2; pie-1::mCherry::par-6*]) from the Hyman Laboratory (Schonegg et al., 2007). Bob Goldstein (Department of Biology, University of North Carolina, Chapel Hill, NC) provided LP172 {hmr-1 (cp21[hmr-1::gfp+LoxP]) I}. RNAi feeding experiments and embryo fixation were performed as described previously (Stevens and Spang, 2013). qPCR (Fig. S3) was performed as described previously (Solinger and Spang, 2014). The AB:P1 ratio was determined by measuring the area of AB and P1 in the central plane using Fiji.

Immunostaining and FM4-64 staining

HMR-1 and MAGI-1 were detected according to Hadwiger et al. (2010) with modifications from Stevens and Spang (2013). α-HMR-1 (Developmental Studies Hybridoma Bank; DSHB) was diluted 1:10 and α-MAGI-1 1:5000 (Stetak and Hajnal, 2011). FM4-64 staining was performed as described previously (Stevens and Spang, 2013).

Microscopy

Images were acquired with a Zeiss Axioplan 2 microscope equipped with a Zeiss Axio Cam MRm camera (Carl Zeiss, Aalen Oberkochen, Germany) and a Plan Apochromat 63× NA 1.40 objective. Images were processed with ImageJ 2.0.0 (Fiji).

Acknowledgements

We thank A. Stetak, A. A. Hyman, B. Goldstein, the DSHB at the University of Iowa and the CGC for strains and reagents.

Competing interests

The authors declare no competing or financial interests.

Author contributions

Conceptualization, A.S. and J.S.; Investigation, J.S.; Formal Analysis, J.S.; Writing, A.S. and J.S.; Supervision, A.S.; Funding Acquisition, A.S.

Funding

This project was supported by the Schweizerischer Nationalfonds zur Förderung der Wissenschaftlichen Forschung (Swiss National Science Foundation) (31003A_141207, 310030B_163480) and the Universität Basel.

Supplementary information

Supplementary information available online at
http://jcs.biologists.org/lookup/doi/10.1242/jcs.189316.supplemental

References

Bossinger, O. and Schierenberg, E. (1992). Cell-cell communication in the embryo of Caenorhabditis elegans. *Dev. Biol.* **151**, 401-409.
Brenner, S. (1974). The genetics of Caenorhabditis elegans. *Genetics* **77**, 71-94.
Costa, M., Raich, W., Agbunag, C., Leung, B., Hardin, J. and Priess, J. R. (1998). A putative catenin-cadherin system mediates morphogenesis of the Caenorhabditis elegans embryo. *J. Cell Biol.* **141**, 297-308.
Goehring, N. W., Hoege, C., Grill, S. W. and Hyman, A. A. (2011). PAR proteins diffuse freely across the anterior-posterior boundary in polarized C. elegans embryos. *J. Cell Biol.* **193**, 583-594.
Hadwiger, G., Dour, S., Arur, S., Fox, P. and Nonet, M. L. (2010). A monoclonal antibody toolkit for C. elegans. *PLoS ONE* **5**, e10161.
Hillier, L. W., Reinke, V., Green, P., Hirst, M., Marra, M. A. and Waterston, R. H. (2009). Massively parallel sequencing of the polyadenylated transcriptome of C. elegans. *Genome Res.* **19**, 657-666.
Jantsch-Plunger, V. and Glotzer, M. (1999). Depletion of syntaxins in the early Caenorhabditis elegans embryo reveals a role for membrane fusion events in cytokinesis. *Curr. Biol.* **9**, 738-745.
Kemphues, K. J., Priess, J. R., Morton, D. G. and Cheng, N. S. (1988). Identification of genes required for cytoplasmic localization in early C. elegans embryos. *Cell* **52**, 311-320.
Klompstra, D., Anderson, D. C., Yeh, J. Y., Zilberman, Y. and Nance, J. (2015). An instructive role for C. elegans E-cadherin in translating cell contact cues into cortical polarity. *Nat. Cell Biol.* **17**, 726-735.
Marston, D. J., Higgins, C. D., Peters, K. A., Cupp, T. D., Dickinson, D. J., Pani, A. M., Moore, R. P., Cox, A. H., Kiehart, D. P. and Goldstein, B. (2016). MRCK-1 drives apical constriction in C. elegans by linking developmental patterning to force generation. *Curr. Biol.* **26**, 2079-2089.
Motegi, F. and Seydoux, G. (2013). The PAR network: redundancy and robustness in a symmetry-breaking system. *Philos. Trans. R. Soc. Lond. B Biol. Sci.* **368**, 20130010.
Munro, E., Nance, J. and Priess, J. R. (2004). Cortical flows powered by asymmetrical contraction transport PAR proteins to establish and maintain anterior-posterior polarity in the early C. elegans embryo. *Dev. Cell* **7**, 413-424.
Panbianco, C., Weinkove, D., Zanin, E., Jones, D., Divecha, N., Gotta, M. and Ahringer, J. (2008). A casein kinase 1 and PAR proteins regulate asymmetry of a PIP(2) synthesis enzyme for asymmetric spindle positioning. *Dev. Cell* **15**, 198-208.
Rappleye, C. A., Paredez, A. R., Smith, C. W., McDonald, K. L. and Aroian, R. V. (1999). The coronin-like protein POD-1 is required for anterior-posterior axis formation and cellular architecture in the nematode caenorhabditis elegans. *Genes Dev.* **13**, 2838-2851.
Schierenberg, E. and Wood, W. B. (1985). Control of cell-cycle timing in early embryos of Caenorhabditis elegans. *Dev. Biol.* **107**, 337-354.
Schmutz, C., Stevens, J. and Spang, A. (2007). Functions of the novel RhoGAP proteins RGA-3 and RGA-4 in the germ line and in the early embryo of C. elegans. *Development* **134**, 3495-3505.
Schonegg, S., Constantinescu, A. T., Hoege, C. and Hyman, A. A. (2007). The Rho GTPase-activating proteins RGA-3 and RGA-4 are required to set the initial size of PAR domains in Caenorhabditis elegans one-cell embryos. *Proc. Natl. Acad. Sci. USA* **104**, 14976-14981.
Solinger, J. A. and Spang, A. (2014). Loss of the Sec1/Munc18-family proteins VPS-33.2 and VPS-33.1 bypasses a block in endosome maturation in Caenorhabditis elegans. *Mol. Biol. Cell* **25**, 3909-3925.
Sönnichsen, B., Koski, L. B., Walsh, A., Marschall, P., Neumann, B., Brehm, M., Alleaume, A. M., Artelt, J., Bettencourt, P., Cassin, E. et al. (2005). Full-genome RNAi profiling of early embryogenesis in Caenorhabditis elegans. *Nature* **434**, 462-469.
Stetak, A. and Hajnal, A. (2011). The C. elegans MAGI-1 protein is a novel component of cell junctions that is required for junctional compartmentalization. *Dev. Biol.* **350**, 24-31.
Stevens, J. and Spang, A. (2013). N-glycosylation is required for secretion and mitosis in C. elegans. *PLoS ONE* **8**, e63687.

Journal of Cell Science

Journal of Cell Science (2017) 130, 1224-1231 doi:10.1242/jcs.189316

Strome, S., Powers, J., Dunn, M., Reese, K., Malone, C. J., White, J., Seydoux, G. and Saxton, W. (2001). Spindle dynamics and the role of gamma-tubulin in early Caenorhabditis elegans embryos. *Mol. Biol. Cell* **12**, 1751-1764.

Várnai, P., Lin, X., Lee, S. B., Tuymetova, G., Bondeva, T., Spät, A., Rhee, S. G., Hajnoczky, G. and Balla, T. (2002). Inositol lipid binding and membrane localization of isolated pleckstrin homology (PH) domains. Studies on the PH domains of phospholipase C delta 1 and p130. *J. Biol. Chem.* **277**, 27412-27422.

Wang, H., Spang, A., Sullivan, M. A., Hryhorenko, J. and Hagen, F. K. (2005). The terminal phase of cytokinesis in the Caenorhabditis elegans early embryo requires protein glycosylation. *Mol. Biol. Cell* **16**, 4202-4213.

Supplemental Movies

Movie 1: Time-lapse movie of a mock RNAi-treated HMR-1::GFP embryo at the second cell division, DIC channel.
Embryo was imaged under pressure-free, isosmotic conditions. Images were taken every 30 seconds.

Journal of Cell Science • Supplementary information

Movie 2: Time-lapse movie of a mock RNAi-treated HMR-1::GFP embryo at the second cell division, GFP channel.
Embryo was imaged under pressure-free, isosmotic conditions. Images were taken every 30 seconds.

Journal of Cell Science • Supplementary information

Movie 3: Time-lapse movie of a ribo-1(RNAi)-treated HMR-1::GFP embryo at the second cell division, DIC channel.
Embryo was imaged under pressure-free, isosmotic conditions. Images were taken every 30 seconds.

Journal of Cell Science • Supplementary information

Movie 4: Time-lapse movie of a ribo-1(RNAi)-treated HMR-1::GFP embryo at the second cell division, GFP channel.
Embryo was imaged under pressure-free, isosmotic conditions. Images were taken every 30 seconds.

Journal of Cell Science • Supplementary information

Movie 5: Time-lapse movie of a ribo-1(RNAi)-treated HMR-1::GFP embryo at the second cell division, DIC channel.
Embryo was imaged under pressure-free, isosmotic conditions. Images were taken every 30 seconds.

Journal of Cell Science • Supplementary information

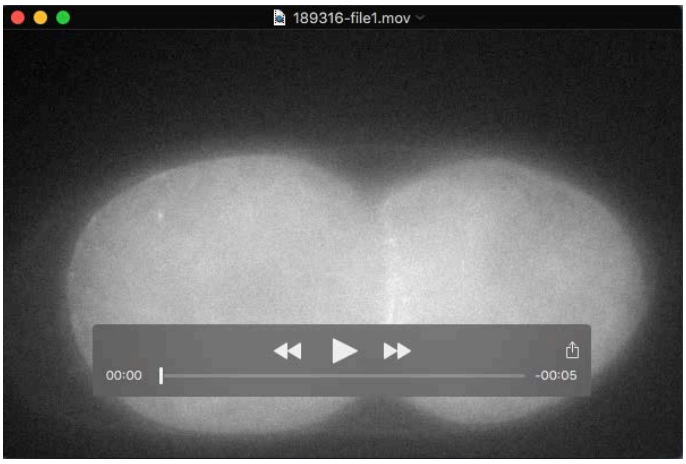

Movie 6: Time-lapse movie of a ribo-1(RNAi)-treated HMR-1::GFP embryo at the second cell division, GFP channel.
Embryo was imaged under pressure-free, isosmotic conditions. Images were taken every 30 seconds.

Journal of Cell Science • Supplementary information

Movie 7: Z-stack of the ribo-1(RNAi)-treated HMR-1::GFP embryo shown in movies 5 and 6, DIC channel.
Embryo was imaged under pressure-free, isosmotic conditions. Distance between Z planes is 1 μm.

Journal of Cell Science • Supplementary information

Movie 8: Z-stack of the ribo-1(RNAi)-treated HMR-1::GFP embryo shown in movies 5 and 6, GFP channel.
Embryo was imaged under pressure-free, isosmotic conditions. Distance between Z planes is 1 μm.

Journal of Cell Science • Supplementary information

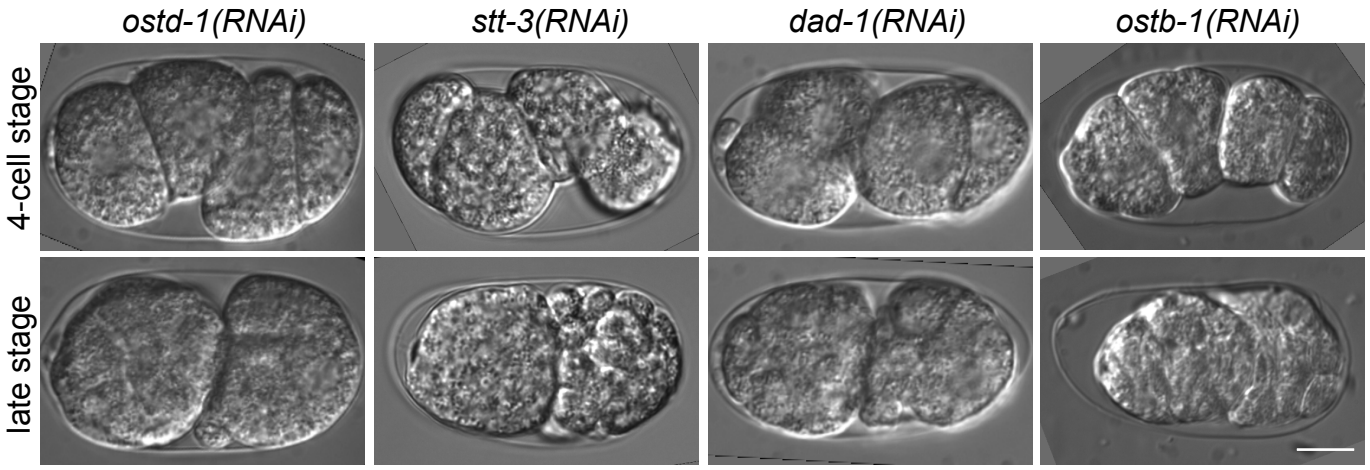

Fig. S1
Knockdown of other OST genes leads to similar phenotypes as ribo-1(RNAi).
DIC images of live embryos taken under pressure-free conditions show the adhesion defect at the 4-cell and multicellular stage. Scalebar: 10 µm.

Journal of Cell Science • Supplementary information

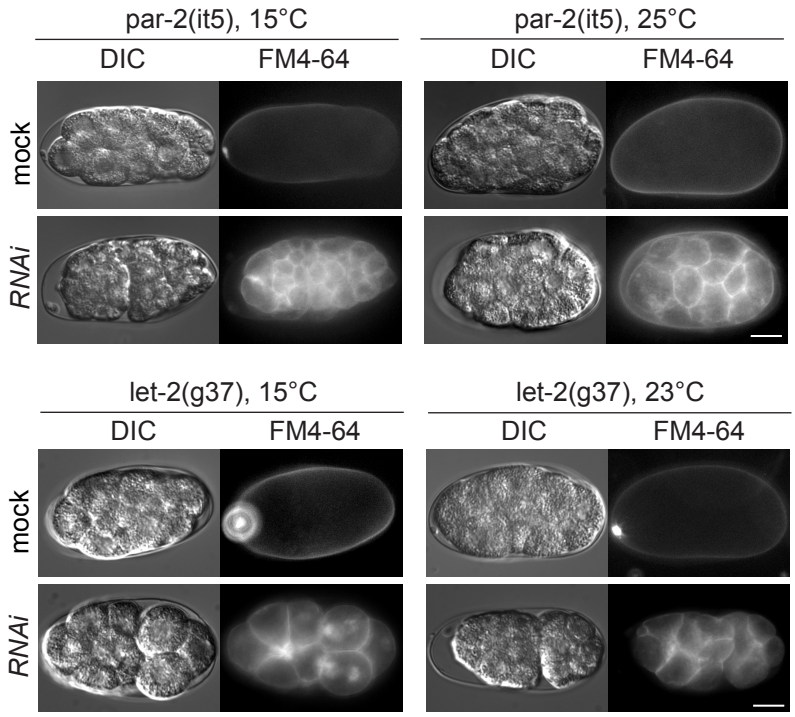

Fig. S2 Examples of multicellular embryos of *ribo-1(RNAi)* treated ts-mutants.

The cleft is visible in *par-2(it5)* only at permissive temperature, while in *let-2(g37)* embryos are clefted irrespective of the temperature.

Journal of Cell Science • Supplementary information

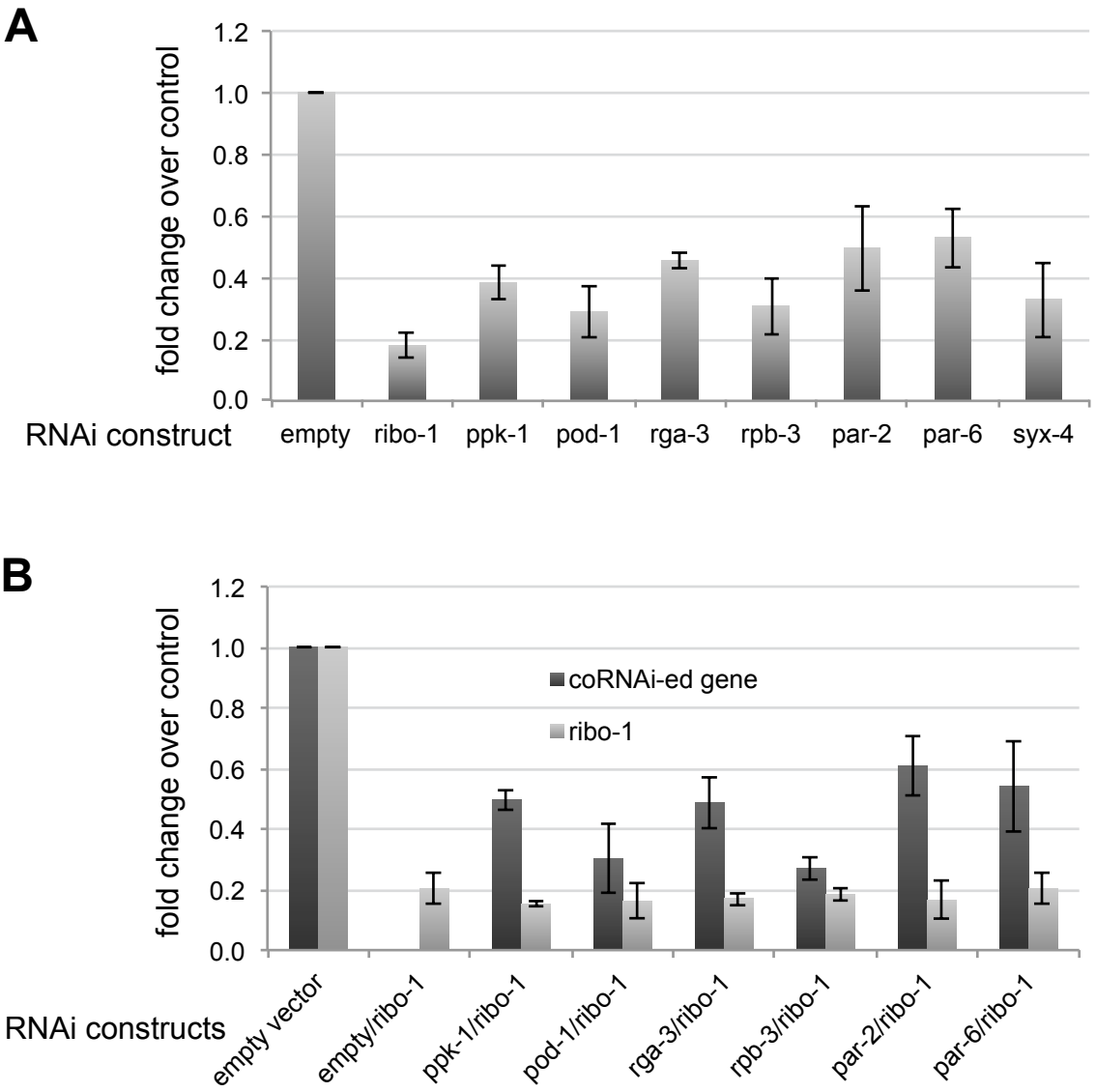

Fig. S3: qPCR verification of the knockdown efficiencies in single (A) and double (B) RNAi feedings.
Total RNA was isolated from adult worms after 36 hours of feeding, the mRNA was reverse transcribed using oligo(dT)15-primers. qPCR was performed using specific primers for the genes of interest, and their levels were analyzed relative to their level in the mock RNAi sample.

Journal of Cell Science • Supplementary information

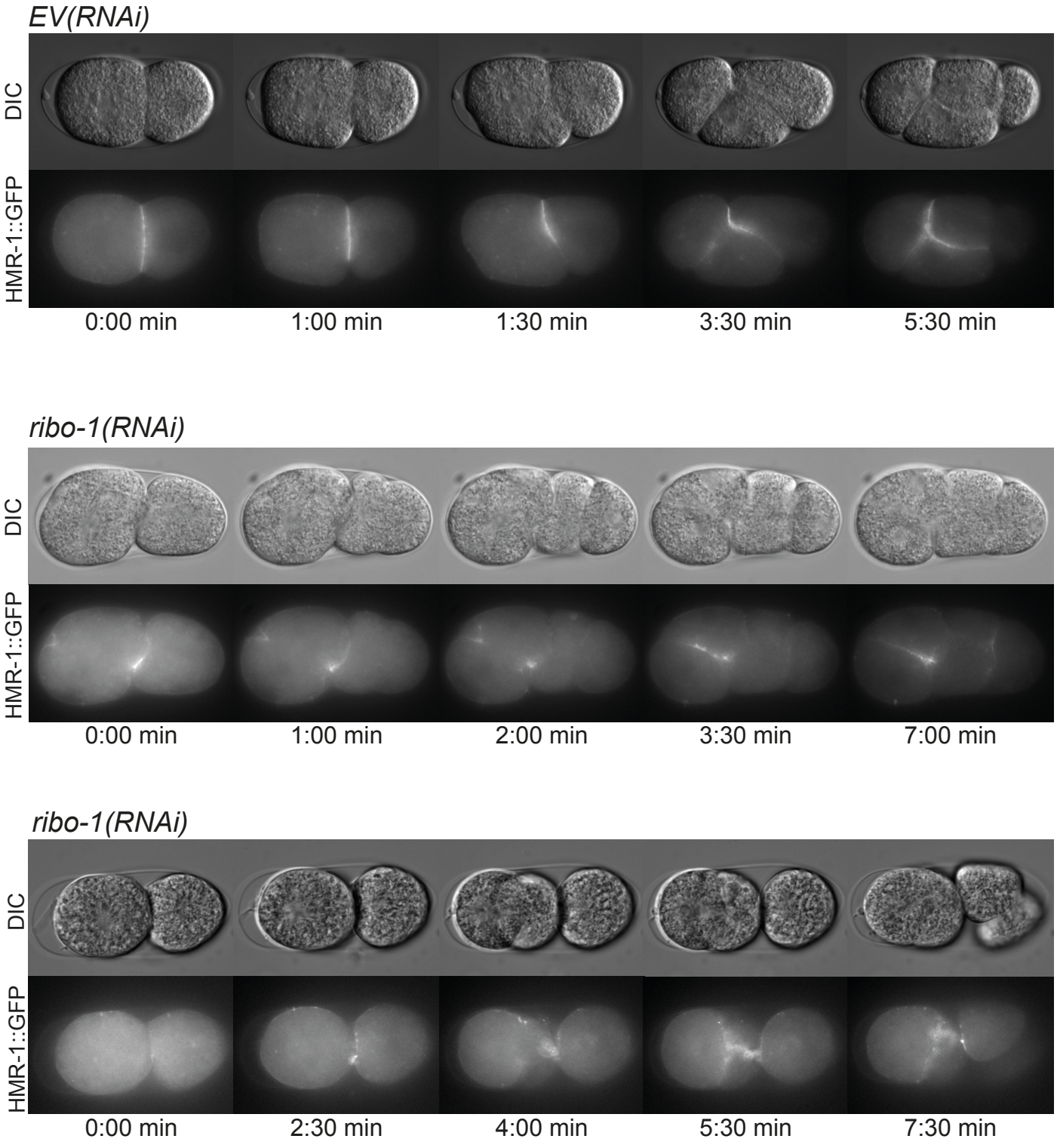

Fig. S4: Stills from time-lapse movies of HMR-1::GFP expressing embryos at the second cell division.
Embryos were imaged under pressure-free, isosmotic conditions. Images were taken every 30 seconds.

Journal of Cell Science • Supplementary information